11-10-2004

Supermassive Black Holes in Active Galactic Nuclei. II. Calibration of the Black Hole Mass-Velocity Dispersion Relationship for Active Galactic Nuclei

Christopher A. Onken
Ohio State University

Laura Ferrarese
Rutgers University

David Merritt
Rochester Institute of Technology

Bradley M. Peterson
Ohio State University

Richard W. Pogge
Ohio State University

See next page for additional authors

Follow this and additional works at: http://scholarworks.rit.edu/article

Authors

Christopher A. Onken, Laura Ferrarese, David Merritt, Bradley M. Peterson, Richard W. Pogge, Marianne Vestergaard, and Amri Wandel

Supermassive Black Holes in Active Galactic Nuclei. II. Calibration of the M_{BH}–$\boldsymbol{\sigma_*}$ Relationship for AGNs

Christopher A. Onken[1], Laura Ferrarese[2], David Merritt[2,3], Bradley M. Peterson[1],
Richard W. Pogge[1], Marianne Vestergaard[1,4], and Amri Wandel[5]

ABSTRACT

We calibrate reverberation-based black hole masses in active galactic nuclei (AGNs) by using the correlation between black hole mass, M_{BH}, and bulge/spheroid stellar velocity dispersion, σ_*. We use new measurements of σ_* for 6 AGNs and published velocity dispersions for 10 others, in conjunction with improved reverberation mapping results, to determine the scaling factor required to bring reverberation-based black hole masses into agreement with the quiescent galaxy M_{BH}–σ_* relationship. The scatter in the AGN BH masses is found to be less than a factor of 3. The current observational uncertainties preclude use of the scaling factor to discriminate between broad-line region models.

Subject headings: galaxies: active — galaxies: nuclei — galaxies: Seyfert

1. INTRODUCTION

The advent of techniques for measuring masses of supermassive black holes (BHs) has led to the identification of correlations between the BH mass (M_{BH}) and various properties of the host galaxies. One of the tightest of these relationships is with the velocity dispersion of the bulge or spheroid (σ_*; Ferrarese & Merritt 2000; Gebhardt et al. 2000a). The objects defining the initial M_{BH}–σ_* relationship were primarily quiescent galaxies, with M_{BH} determined from stellar kinematics or gas dynamics. However, galaxies hosting an active galactic nucleus (AGN), in which the BH mass was measured via reverberation mapping (Blandford & McKee 1982; Peterson 1993),

---

[1]Department of Astronomy, The Ohio State University, 140 West 18th Avenue, Columbus, OH 43210; onken, peterson, pogge@astronomy.ohio-state.edu

[2]Department of Physics and Astronomy, Rutgers University, 136 Frelinghuysen Road, Piscataway, NJ 08854; lff@physics.rutgers.edu

[3]Current address: Department of Physics, Rochester Institute of Technology, 84 Lomb Memorial Drive, Rochester, NY 14623; drmsps@rit.edu

[4]Current address: Steward Observatory, University of Arizona, 933 North Cherry Avenue, Tucson, AZ 85721; mvestergaard@as.arizona.edu

[5]Racah Institute, Hebrew University, Jerusalem 91904, Israel; amri@vms.huji.ac.il

have been found to be consistent with following the same correlation (Gebhardt et al. 2000b; Ferrarese et al. 2001 [hereafter Paper I]; Onken et al. 2003).

The values of $M_{\rm BH}$ derived from reverberation mapping are subject to certain systematic uncertainties. In tracing the response of gas in the broad-line region (BLR) to the variable ionizing continuum of the AGN, the time delay between the fluctuations in the continuum and the "reverberation" of the BLR emission lines gives a characteristic radius of the BLR gas, r. The orbital velocity at that radius is estimated by the width, ΔV, of the emission line (specifically, the variable part of the line). But the kinematics and geometry of the BLR introduces a scaling factor, f, into the reverberation mass equation:

$$M_{\rm BH} = f\ \frac{r\ \Delta V^2}{G}. \tag{1}$$

Simple models of BLR morphologies yield f parameters on the order of unity, and the application of such estimates, as in the above references, places the previous AGN $M_{\rm BH}$–σ_* data among the locus of quiescent galaxies.

A uniform relationship between the BH mass and properties of the host galaxy on size scales beyond the strong gravitational influence of the BH implies a causal connection between the formation of the galaxy and the central black hole. Many investigators have explored possible mechanisms for how the evolution of the BH and galaxy could be linked (e.g., Silk & Rees 1998; Haehnelt & Kauffmann 2000; Adams, Graff, & Richstone 2001; Umemura 2001; Miralda-Escudé & Kollmeier 2003; Merritt & Poon 2004), while others have looked for outliers from these relationships as probes of the physical drivers of the correlations (e.g. Mathur, Kuraszkiewicz, & Czerny 2001; Wandel 2002; Bian & Zhao 2004; Grupe & Mathur 2004).

We present measurements of stellar velocity dispersions for 6 reverberation-mapped AGNs, significantly enlarging the sample of objects which can be used to observationally investigate the $M_{\rm BH}$–σ_* relationship for active galaxies. In §2, we describe our observations and analysis method. We present our results and discuss the implications for the ensemble average value of the reverberation mapping scaling factor, $\langle f \rangle$, in §3. Our conclusions are summarized in §4.

2.   OBSERVATIONS AND DATA REDUCTION

The velocity dispersions for our sample of AGNs were measured using the near-infrared Ca II triplet (CaT). These stellar absorption lines, at rest wavelengths of λ8498, 8542, and 8662 Å, occur in a region of relatively low AGN contribution (Nelson & Whittle 1995), and are accessible to ground-based observations for sources with redshift $z \lesssim 0.068$ (water vapor bands begin to reduce atmospheric transparency at longer wavelengths).

Observations were conducted at Kitt Peak National Observatory (KPNO), Cerro Tololo Inter-American Observatory (CTIO), and MDM Observatory. The general observing strategy at each of the telescopes was similar. Long-slit spectra of each target were bracketed by quartz-lamp

flat fields and wavelength calibration exposures. The total exposure time for each AGN typically exceeded 10,000 seconds. In addition to our targets, we obtained spectra of late-type giant stars (G8 III–K6 III) to use as spectral templates. Details of the observing runs are given below and in Table 1.

KPNO Observations. We observed at the Mayall 4 m telescope with the Ritchey-Chrétien (R-C) Spectrograph. The BL380 grating (1200 lines mm^{-1}, blazed at 9000 Å) was used with an RG695 blocking filter and the LB1A CCD. The slit width was 2″, with a dispersion of 0.45 Å pixel^{-1} and a wavelength range of 8250–9130 Å.

CTIO Observations. We used the V.M. Blanco 4 m telescope with the R-C Spectrograph, equipped with the KPGLD-1 grating (790 lines mm^{-1}, blazed at 8500 Å) and an RG665 filter. We used the lower right amplifier for the Loral 3K 1 CCD detector within a window of 3072×585 pixels. The reduced spectra have a dispersion of 0.83 Å pixel^{-1} over a wavelength range of 7500–10060 Å. The slit dimensions were 2×344″.

MDM Observations. Our first observations at the MDM 2.4 m telescope were made with the MDM Observatory Modular Spectrograph (ModSpec), using a grating of 830.8 lines mm^{-1}, blazed at 8465 Å. The OG515 order-separating filter was used. The detector for these observations was "Charlotte", a thinned, backside-illuminated, SITe 1024×1024 CCD. The spectra covered a range of ∼1400 Å, with a dispersion of about 1.43 Å pixel^{-1}, and a slit width of approximately 2″. The second MDM observing run used the ModSpec setup described above, but utilized a different detector. "Echelle", a thinned, backside-illuminated, SITe 2048×2048 CCD was used with a windowing of 330×2048 pixels.

2.1. Data Reduction and Analysis

We used IRAF[1] and XVista[2] for the reduction of different subsets of the data. However, the basic strategy was the same: the spectra were flat-fielded, sky-subtracted, and placed on a linear wavelength scale.

The AGN spectra in our sample were often contaminated by the broad O I $\lambda8446$ emission line that appears blueward of the CaT, and these lines were removed with a high order polynomial

---

[1]IRAF is distributed by the National Optical Astronomy Observatories, which are operated by the Association of Universities for Research in Astronomy, Inc., under cooperative agreement with the National Science Foundation

[2]See http://ganymede.nmsu.edu/holtz/xvista

in order to isolate the CaT absorption lines. None of our objects show evidence of emission from high-order Paschen emission lines, which can also contaminate the CaT lines.

3. RESULTS AND DISCUSSION

3.1. Measuring Velocity Dispersions

We measured the velocity dispersions from the reduced spectra with the Fourier correlation quotient method (FCQ; Bender 1990). Cross-correlating the galaxy spectra with those of the template stars produces values for the central velocity dispersions.

Our galaxy spectra and the best template-star fits from the FCQ routine are shown in Figure 1. The results of our velocity dispersion analysis are listed in Table 2. As noted in Paper I, the formal errors reported by the FCQ fitting routine tend to underestimate the total uncertainties for the σ_* measurements. Thus, in cases where the FCQ output errors were smaller than 15%, the error bars have been brought up to this threshold.

Based on visual inspection, the least satisfactory fit from Figure 1 is that of Akn 120. However, consistent (within 1 σ) results are found from three other methods: (1) a simple Gaussian fit to the strongest absorption line; (2) the second moment of the profile for that line; and (3) an IDL routine for penalized pixel fitting[3].

We examined whether the AGN continuum could dilute the stellar absorption lines in a manner that would affect the σ_* measurements. This was tested by artificially including an additional continuum contribution and running the FCQ routine again. Over a large range of continuum levels, no significant change was seen in the resulting σ_* values.

Additional stellar velocity dispersion data for galaxies hosting AGNs have been taken from the literature.

3.2. Measuring Virial Products

New analysis of reverberation mapping data has produced updated measurements of the virial products ($r \, \Delta V^2/G$) for a sample of 35 AGNs, including the 16 which now have velocity dispersions (Peterson et al. 2004). These virial products, which, from equation (1), can also be written as M_{BH}/f, differ from the majority of previous reverberation mapping analyses in the calculation of ΔV. Whereas earlier work typically characterized the velocity width via the full-width at half-maximum (FWHM) of the emission line, Peterson et al. (2004) have found more consistent virial products when using the line dispersion (i.e., the second moment of the line profile; σ_{line}) instead.

---

[3]See Cappellari & Emsellem (2004), and http://www.strw.leidenuniv.nl/~mcappell/idl/ for details.

This will have important implications for comparing our results with previous publications.

3.3. The $M_{\rm BH}$–σ_* Relation

We assume that the $M_{\rm BH}$–σ_* correlation found in quiescent galaxies also holds for AGNs and their host galaxies. We can then determine the factor required to scale the AGN virial products $(M_{\rm BH}/f)$ to the quiescent galaxy relation (holding σ_* fixed at the measured value); that is, we calculate the average scaling factor, $\langle f \rangle$, that, when multiplied by the virial products, brings the AGN $M_{\rm BH}$–σ_* relation into agreement with the quiescent galaxy relationship.

Because published determinations of the slope of the quiescent galaxy relation have yet to converge, we selected the most prominent slope values from either end of the quoted range. Thus, we consider both the Tremaine et al. (2002; hereafter T02) slope of 4.02, and the Ferrarese (2002; F02, henceforth) slope of 4.58, and determine separate scaling factors, $\langle f_{\rm T} \rangle$ and $\langle f_{\rm F} \rangle$, respectively.

While questions remain as to the reliability of the current fits to the quiescent galaxy $M_{\rm BH}$–σ_* relation, especially with respect to the accuracy of the black hole masses from stellar kinematics (see Valluri, Merritt, & Emsellem 2004; Cretton & Emsellem 2004; Richstone et al. 2004), we hope our use of the two slope values will give a more reliable estimate of the uncertainties involved while also avoiding entanglement in the continuing controversy.

The best fit to the AGN $M_{\rm BH}$–σ_* values was accomplished with the orthogonal regression program, GaussFit[4] (version 3.53; Jefferys, Fitzpatrick, & McArthur 1988), which accounts for errors in both $(M_{\rm BH}/f)$ and σ_*. For the purposes of our GaussFit analysis, the asymmetric variances in the virial products were symmetrized as the mean of the upper and lower variances. A fit was made to the equation

$$\log\left(\frac{M_{\rm BH}}{f}\right) = \alpha + \beta \, \log\left(\frac{\sigma_*}{200}\right) \;, \tag{2}$$

where α is the normalization of the relationship, β is the (fixed) value of the slope, and where $(M_{\rm BH}/f)$ is in solar masses and σ_* is in km s^{-1}. For each slope, the best-fit value of α was calculated. The χ^2 which was minimized to determine the best fit is given by

$$\chi^2 \equiv \sum_{i=1}^{N} \frac{\left[(\frac{M_{\rm BH}}{f})_i - \alpha - \beta(\frac{\sigma_*}{200})_i\right]^2}{\sigma_{Mi}^2 + \beta^2 \sigma_{\sigma i}^2} \;, \tag{3}$$

where $\sigma_{{\rm M}i}$ and $\sigma_{\sigma i}$ are the uncertainties in the virial product and the velocity dispersion, respectively, for the ith data pair (Press et al. 1992). The virial products and velocity dispersions used in our fits are given in Table 3.

---

[4] GaussFit is available at ftp://clyde.as.utexas.edu/pub/gaussfit/

The published values of the quiescent galaxy intercept correspond to $\alpha_F = 8.22\pm0.08$ and $\alpha_T = 8.13\pm0.06$. Our fits with fixed slopes are shown in Figure 2, and yield $\alpha_F^{AGN} = 7.48\pm0.13$ and $\alpha_T^{AGN} = 7.39\pm0.12$. Remarkably, both slopes give the same best fit value, $\log\langle f \rangle = 0.74$. Hence, $\langle f_F \rangle = 5.5\pm1.9$ and $\langle f_T \rangle = 5.5\pm1.7$. The χ^2 per degree of freedom, χ_ν^2, for these two fits are 2.90 and 2.87, respectively.

Table 4 shows the resulting α and β values for a variety of fitting constraints. When we allow β to vary in the fit to the AGNs, the result is consistent with both the T02 and F02 slopes, albeit with a large uncertainty. The distribution of points with previous σ_* measurements in Figure 2 differs from that of Paper I because of the improved virial product data from Peterson et al. (2004).

Because the reverberation mapping results for IC 4329A and NGC 4593 provide only upper limits on the black hole masses, these data were omitted from the above analysis. The formal error bars on $M_{\rm BH}$ can extend below zero because the uncertainty of the time delay is not restricted to positive values. If we take the uncertainty in $\log M_{\rm BH}$ to be $\sigma_{\rm M}/(M \ln 10)$, we can avoid taking the logarithms of negative numbers, and these two data points can be included in the fit. The uncertainties are large enough, however, that the fit is not changed in a statistically significant way. Additionally, the fit is not strongly affected by the exclusion of NGC 4051 (see Table 4), which seems to be an outlier in the AGN radius-luminosity relationship (see the Appendix of Vestergaard 2002). When we do not include NGC 4051, we find $\langle f_F \rangle = 5.1$ and $\langle f_T \rangle = 5.2$, differences of less than 8% from our best fit value of 5.5.

The most common assumption for converting a virial product to $M_{\rm BH}$ is that of Netzer (1990)

$$M_{\rm BH} = \frac{3\ r\ V_{\rm FWHM}^2}{4\ G}, \tag{4}$$

which implicitly assumes an isotropic velocity distribution and $\Delta V = V_{\rm FWHM} / 2$, where $V_{\rm FWHM}$ is the line full width at half maximum. Peterson et al. (2004) measure the second moment of the line profile, $\sigma_{\rm line}$, rather than $V_{\rm FWHM}$, so an isotropic velocity field simply gives $f = 3$ with no other assumptions. Denoting the scale factor as ϵ when using $V_{\rm FWHM}$ and f when using $\sigma_{\rm line}$, we find that whereas Netzer's assumptions give $\epsilon = 0.75$ (as in eq. [4]), the value of $\langle f \rangle$ we derive above implies $\langle \epsilon \rangle = 1.4$, i.e., black hole masses $\sim$1.8 times higher[5]. Our masses are only 62% as large as those expected from the $\sigma_{\rm line}$–$V_{\rm FWHM}$ relation found in a model-dependent fit to the distribution of $V_{\rm FWHM}$ in a sample of quasars and Seyfert galaxies (McLure & Dunlop 2001).

Applying our derived value of $\langle f \rangle = 5.5$ (or $\langle \epsilon \rangle = 1.4$) will remove the systematic bias between the virial product and mass of the black hole (modulo the accuracy of the particular $M_{\rm BH}$–σ_* fit chosen). Yet, estimates for individual AGN black hole masses may fall substantially off the $M_{\rm BH}$–σ_* relation, as there are still rms deviations from the fits in the mass direction of factors of 2.9 (F02 slope) and 2.6 (T02 slope).

---

[5]Our value of ϵ is calculated assuming $\sigma_{\rm line} = V_{\rm FWHM}/2$; for typical line profiles, changing the shape of the line alters the $\sigma_{\rm line}$–$V_{\rm FWHM}$ conversion by an amount smaller than the observed scatter in the $M_{\rm BH}$–σ_* data.

Whether the scatter in $M_{\rm BH}$ is due to differences in the BLR properties in each AGN (corresponding to slightly different f values for each object) or a problem in our assumption that all AGNs fall on the quiescent galaxy relationship remains unclear. However, models of the BLR may shed light on this question.

3.4.   BLR Models

Given our determination of $\langle f \rangle$, we can try to learn something about the structure and kinematics of the BLR. Modeling of the BLR, taking into account different radial profiles and discrete time sampling of example light curves, will be undertaken in a later paper. Here we describe only a thin, rotating ring. In this case, f can be thought of as relating the Keplerian velocity ($V_{\rm rot}$) at the radius of the ring (which is traced by the appropriate time delay) to the observed line dispersion:

$$f = \left(\frac{V_{\rm rot}}{\sigma_{\rm line}}\right)^2,\tag{5}$$

For a ring of inclination i (where $i{=}0°$ for face-on), this model gives $f = 2\ln 2 \, / \sin^2 i$.

Working within a thin-ring model context, Wu & Han (2001) calculated the inclinations necessary to scale published reverberation mapping results for 11 AGNs to the quiescent galaxy $M_{\rm BH}$–σ_* relation. With our revised virial product results, we find that this very simple model fails for two of our 16 AGNs. NGC 3783 and Mrk 110 would require $\sin i$ values greater than unity to scale them to the quiescent galaxy $M_{\rm BH}$–σ_* relation. For our other sources, we do not find any evidence to support the inclination trends with line width or radio loudness that were claimed by Wu & Han. Further constraints on the BLR geometry are not feasible given the sizes of the current uncertainties.

3.5.   Gravitational Redshifts

In principle, an independent measure of the AGN black hole mass can be obtained by detection of gravitational redshifting of the emission lines (e.g., Netzer 1977; Peterson et al. 1984). Kollatschny (2003b) finds that the variable parts of the strong broad lines in the optical spectrum of Mrk 110 are redshifted relative to the systemic velocity. The reverberation time lag and redshift of each line relative to systemic are anticorrelated and appear to be consistent with a gravitational redshift caused by a central mass $M_{\rm grav} \approx 1.4 \times 10^8 \, M_\odot$, rather higher than our reverberation-based mass[6] (Table 3) of $M_{\rm BH} = 2.5 \times 10^7 \, M_\odot$.

---

[6]Kollatschny (2003a) obtains a reverberation-based mass estimate of $1.8 \times 10^7 \, M_\odot$, but using FWHM as the linewidth measure and $\epsilon = 1.5$ (see §3.1). The FWHM data of Peterson et al. (2004) gives a result consistent with that of Kollatschny, however our preferred method of measuring $\sigma_{\rm line}$ and using the empirical calibration of $\langle f \rangle$ yields a black hole mass approximately 40% larger.

Regardless of the particular value of f appropriate to Mrk 110, the offset between the reverberation-based virial product and the gravitational redshift mass is in the direction expected. However, the value of M_{grav} places Mrk 110 even further above the M_{BH}–σ_* relation, which predicts $M_{\mathrm{BH}} \approx 4 \times 10^6\, M_{\odot}$.

If the BLR is modeled as a simple disk, then

$$\frac{(M_{\mathrm{BH}}/f)}{M_{\mathrm{grav}}} = \frac{\sin^2 i}{2\ln 2}, \tag{6}$$

and the difference between these two measurements allows us to infer that $i \approx 30°$, slightly larger than the 21 ± 5 degrees found by Kollatschny (2003b).

Measuring gravitational redshifts appears to be a promising technique for independently estimating central masses. However, applying the method is non-trivial because the gravitational redshifts are small, typically only several tens to a few hundred kilometers per second. Moreover, it is not a shortcut around reverberation mapping because (a) the redshift must be measured in the variable part of the emission line (i.e., the root-mean-square spectrum formed from the monitoring data; see Peterson et al. 2004) and (b) the time lag, which can vary with time, needs to be measured simultaneously. The spectral resolution required to measure such small redshifts reliably is higher than usually employed in reverberation mapping campaigns, with the exception of Kollatschny's (2003a) program on Mrk 110 and the *Hubble Space Telescope* monitoring program on NGC 5548 (Korista et al. 1995). A re-examination of the NGC 5548 spectra from the latter campaign shows some evidence for redshifts at the expected levels, although the errors are quite large. Additional data will thus be required to examine this method of black hole mass measurement more thoroughly and to determine whether Mrk 110 is truly a significant outlier from the M_{BH}–σ_* relation.

3.6. σ_* Versus FWHM([O III]λ5007 Å)

Several recent studies have suggested the use of the FWHM of the [O III]λ5007 Å emission line as a proxy for σ_*. Nelson & Whittle (1996) examined a sample of 66 Seyfert galaxies with both σ_* and FWHM([O III]) measurements and found scatter of 0.20 dex around a 1:1 correspondence (see their Figures 5 and 7a). Based on these trends, Nelson (2000) and Shields et al. (2003) used [O III] data as a substitute for σ_* in AGNs out to z$\sim$3. Boroson (2003) applied the same arguments to data from the Sloan Digital Sky Survey Early Data Release and found that using FWHM([O III]) could reproduce an M_{BH}–σ_*-like relationship, although with a larger scatter than has been found for quiescent galaxies (i.e., a factor of $\sim$5). Statistically identical distributions in FWHM([O III]) were found for the broad-line and narrow-line Seyfert 1s in an X-ray selected sample of AGNs, which placed the narrow-line Seyfert 1s preferentially below the M_{BH}–σ_* relation (Grupe & Mathur 2004).

With the FWHM([O III]) data tabulated by Nelson (2000) for our 16 AGNs, we looked at the relationship with σ_*. Figure 3 shows that 25% of the sources have FWHM([O III]) data that deviate by $>$0.2 dex from the values expected based on their velocity dispersions. There is no

evidence of the correlation between the discrepant objects and their radio power that was found for a larger sample of Seyferts (Nelson & Whittle 1996), indicating that these differences may not be due to a systematic acceleration of the [O III]-emitting gas by the radio source. Overall, the weighted mean difference from equality is 0.03 dex (in the sense of larger FWHM relative to σ_*) with an rms scatter of 0.15 dex. In the way of commentary, we simply echo sentiments expressed by others that while use of such a proxy may be valid for a large sample of AGNs, it can also fail dramatically for individual objects.

4. CONCLUSION

With the addition of 6 new velocity dispersion measurements for reverberation-mapped AGNs and making use of improved reverberation mapping results, we tie together the $M_{\rm BH}$–σ_* relationships for quiescent galaxies and AGNs. This allows us to calculate the average scaling factor, $\langle f \rangle$, which removes the statistical bias between the virial product generated by reverberation mapping and the black hole mass. For the F02 and T02 fits to the quiescent galaxy $M_{\rm BH}$–σ_* relationship, we find $\langle f \rangle = 5.5 \pm 1.9$ and 5.5 ± 1.7, respectively. These values of $\langle f \rangle$ apply specifically to virial products using the dispersion of the emission lines, rather than measurements of the FWHM. While modeling of the BLR and studies of emission line gravitational redshifts may eventually lead to a better understanding of the structure and kinematics of the BLR, further work is needed.

REFERENCES

Adams, F. C., Graff, D. S., & Richstone, D. O. 2001, ApJ, 551, L31

Arribas, S., Mediavilla, E., Garcia-Lorenzo, B., & del Burgo, C. 1997, ApJ, 490, 227

Bender, R. 1990, A&A, 229, 441

Bian, W., & Zhao, Y. 2004, MNRAS, 347, 607

Blandford, R., & McKee, C. F. 1982, ApJ, 255, 419

Boroson, T. 2003, ApJ, 585, 647

Cappellari, M., & Emsellem, E. 2004, PASP, 116, 138

Cretton, N., & Emsellem, E. 2004, MNRAS, 347, L31

de Vaucouleurs, G., de Vaucouleurs, A., Corwin, H. G., Jr., Buta, R., Paturel, G., & Fouque, P. 1991, Third Reference Catalogue of Bright Galaxies (New York: Springer)

Falco, E. E., et al. 1999, PASP, 111, 438

Ferrarese, L. 2002, in Current High-Energy Emission Around Black Holes, ed. C.-H. Lee & H.-Y. Chang (Singapore: World Scientific), 3 (F02; astro-ph/0203047)

Ferrarese, L., & Merritt, D. 2000, ApJ, 539, L9

Ferrarese, L., Pogge, R. W., Peterson, B. M., Merritt, D., Wandel, A., & Joseph, C. L. 2001, ApJ, 555, L79 (Paper I)

Gebhardt, K., et al. 2000a, ApJ, 539, L13

Gebhardt, K., et al. 2000b, ApJ, 543, L5

Green, R. F., Nelson, C. H., & Boroson, T. 2003, in Carnegie Observatories Astrophysics Series, Vol. 1: Coevolution of Black Holes and Galaxies, ed. L. C. Ho (Pasadena: Carnegie Observatories, http://www.ociw.edu/ociw/symposia/series/ symposium1/proceedings.html)

Grupe, D., & Mathur, S. 2004, ApJ, 606, L41

Haehnelt, M. G., & Kauffmann, G. 2000, MNRAS, 318, L35

Jefferys, W. H., Fitzpatrick, M. J., & McArthur, B. E. 1988, Celes. Mech., 41, 39

Keel, W. C. 1996, ApJS, 106, 27

Kollatschny, W. 2003a, A&A, 407, 461

Kollatschny, W. 2003b, A&A, 412, L61

Korista, K. T., et al. 1995, ApJS, 97, 285

Mathur, S., Kuraszkiewicz, J., & Czerny, B. 2001, NewA, 6, 321

McLure, R. J., & Dunlop, J. S. 2001, MNRAS, 327, 199

Merritt, D., & Poon, M. Y. 2004, ApJ, 606, 788

Miralda-Escudé, J., & Kollmeier, J. A. 2003, ApJ, submitted (astro-ph/0310717)

Nelson, C. H. 2000, ApJ, 544, L91

Nelson, C. H., & Whittle, M. 1995, ApJS, 99, 67

Nelson, C. H., & Whittle, M. 1996, ApJ, 465, 96

Netzer, H. 1977, MNRAS, 181, 89P

Netzer, H. 1990, in Active Galactic Nuclei, ed. R. D. Blandford, H. Netzer, & L. Woltjer (Berlin: Springer), 137

Onken, C. A., Peterson, B. M., Dietrich, M., Robinson, A., & Salamanca, I. M. 2003, ApJ, 585, 121

Peterson, B. M. 1993, PASP, 105, 247

Peterson, B. M., et al. 2004, ApJ, submitted

Peterson, B. M., Meyers, K. A., Capriotti, E. R., Foltz, C. B., Wilkes, B. J., & Miller, H. R. 1984, ApJ, 292, 164

Press, W. H., Teukolsky, S. A., Vetterling, W. T., & Flannery, B. P. 1992, Numerical Recipes (2nd ed.; Cambridge: Cambridge Univ. Press)

Richstone, D., et al. 2004, ApJL, submitted (astro-ph/0403257)

Shields, G. A., Gebhardt, K., Salviander, S., Wills, B. J., Xie, B., Brotherton, M. S., Yuan, J., & Dietrich, M. 2003, ApJ, 583, 124

Silk, J., & Rees, M. J. 1998, A&A, 331, L1

Theureau, G., Bottinelli, L., Coudreau-Durand, N., Gouguenheim, L., Hallet, N., Loulergue, M., Paturel, G., & Teerikorpi, P. 1998, A&AS, 130, 333

Tremaine, S., et al. 2002, ApJ, 574, 740 (T02)

Umemura, M. 2001, ApJ, 560, L29

Valluri, M., Merritt, D., & Emsellem, E. 2004, ApJ, 602, 66

Vestergaard, M. 2002, ApJ, 571, 733

Wandel, A. 2002, ApJ, 565, 762

Willmer, C. N. A., Focardi, P., Chan, R., Pilligrini, P. S., & da Costa, N. L. 1991, AJ, 101, 57

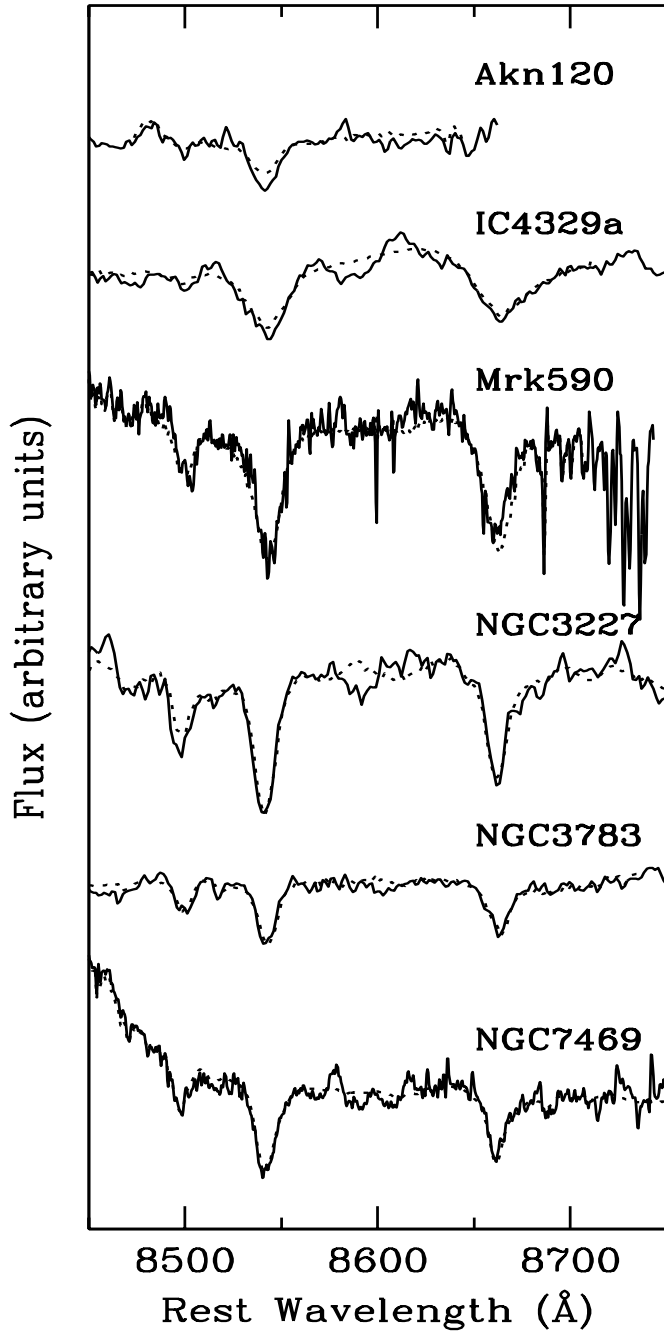Wu, X.-B., & Han, J. L. 2001, ApJ, 561, L59

Fig. 1.— Normalized spectra of the CaT region for the 6 AGNs in this study. Each spectrum has been offset in flux for clarity. The dashed line indicates the best fit obtained with the FCQ method. The spectrum of Akn 120 is truncated where the FCQ fit becomes unstable. The spectra shown for Mrk 590 and NGC 7469 are from KPNO; IC 4329A and NGC 3783 are from MDM.
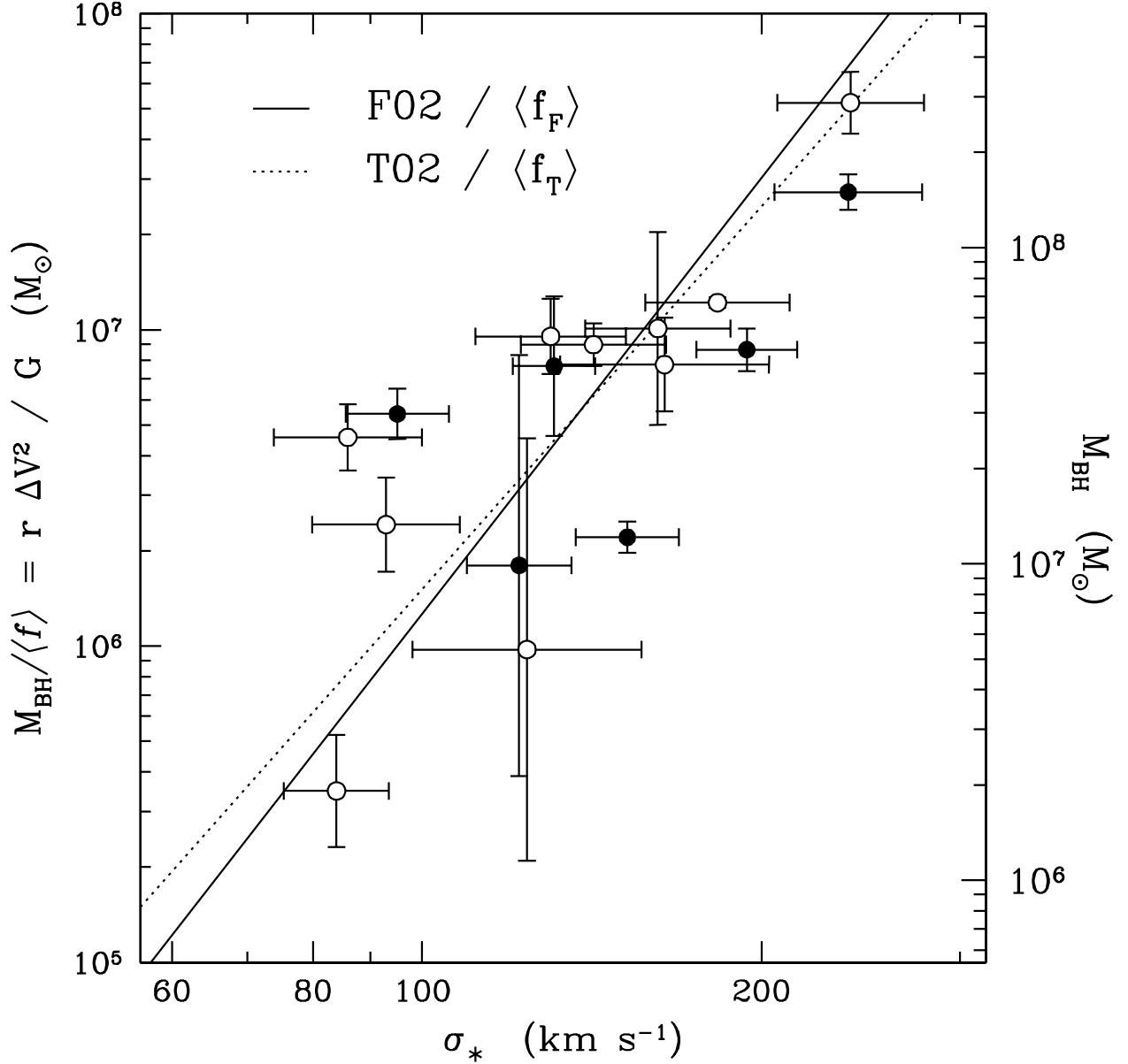
Fig. 2.— Virial product, M_{BH}/f, versus host galaxy velocity dispersion, σ_*. Solid points indicate objects with σ_* measurements presented here. Open points represent AGNs with previously published σ_* data. The solid line indicates the F02 slope of 4.58, with the y-intercept shifted downward by $\langle f_F \rangle$. The dotted line denotes the T02 slope of 4.02, with the y-intercept scaled down by $\langle f_T \rangle$. The vertical scale on the right uses our derived offset: $\langle f_F \rangle = \langle f_T \rangle = 5.5$.
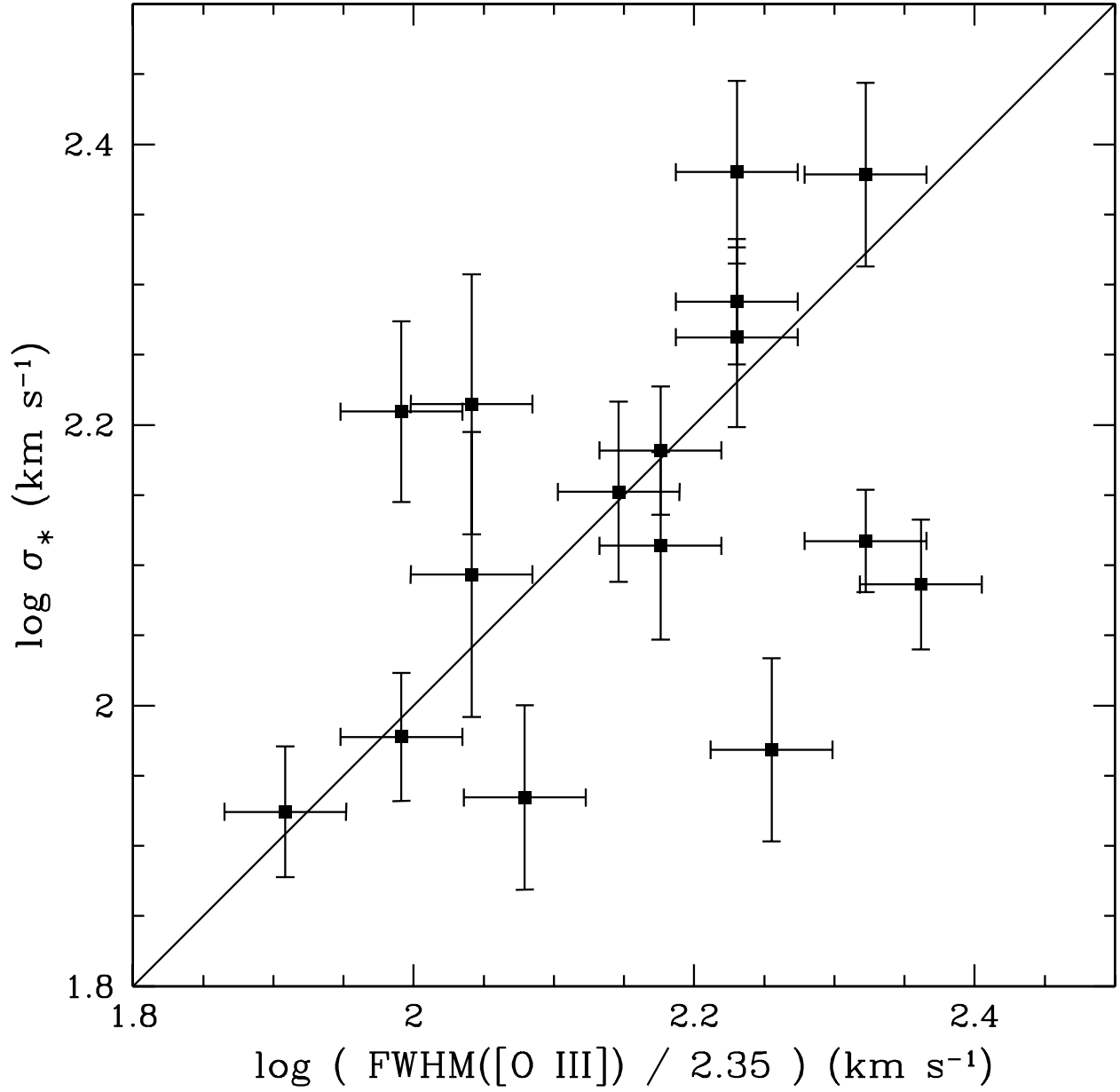
Fig. 3.— σ_* versus FWHM([O III]) for our 16 AGNs. The solid line shows a 1:1 correspondence between σ_* and the equivalent for a Gaussian line profile, FWHM([O III]) / 2.35.

Table 1.   Observing Log

Run	Telescope	Instrument	UT Dates	Resolution (km s^{-1})	Targets Observed
MDM-a	MDM 2.4m	ModSpec	2001 Oct 20–24	95	Mrk 590, NGC 3227, NGC 7469
KPNO	KPNO 4m	R-C Spec	2001 Oct 29–Nov 1	60	Akn 120, Mrk 590, NGC 7469
MDM-b	MDM 2.4m	ModSpec	2003 Mar 12–13	95	IC 4329A, NGC 3783
CTIO	CTIO 4m	R-C Spec	2003 Apr 18	90	IC 4329A, NGC 3783

Table 2.   Velocity Dispersion Measurements

Galaxy	Redshift	Redshift References	Run	σ_* (km s^{-1})
Akn 120	0.032296±0.000143	1	KPNO	239±36
IC 4329A	0.016054±0.000050	2	CTIO	131^{+20}_{-60}
⋯			MDM-b	121±18
Mrk 590	0.026385±0.000040	3	KPNO	201±30
⋯			MDM-a	188±28
NGC 3227	0.003859±0.000010	3	MDM-a	139±21
NGC 3783	0.009730±0.000007	4	CTIO	87±13
⋯			MDM-b	108±16
NGC 7469	0.016317±0.000007	5	KPNO	149±22
⋯			MDM-a	157±24

References. — (1) Falco et al. 1999; (2) Willmer et al. 1991; (3) de Vaucouleurs et al. 1991; (4) Theureau et al. 1998; (5) Keel 1996.

Table 3. M_{BH}–σ_* Data

Galaxy	Virial Product[a] (10^6 M$_\odot$)	Black Hole Mass[b] (10^6 M$_\odot$)	σ_* (avg) (km s^{-1})	σ_* References
3C 120	$10.1^{+5.7}_{-4.1}$	$55.6^{+31.4}_{-22.3}$	162±24	2
3C 390.3	52.2±11.7	289±64	240±36	3
Akn 120	27.2±3.5	150±19	239±36	1
IC 4329A[c]	$1.80^{+3.25}_{-2.16}$	$9.9^{+17.9}_{-11.9}$	122±13	1
Mrk 79	9.52±2.61	52.4±14.4	130±20	4
Mrk 110	4.57±1.10	25.1±6.1	86±13	4
Mrk 590	8.64±1.34	47.5±7.4	194±20	1
Mrk 817	8.98±1.40	49.4±7.7	142±21	4
NGC 3227	7.67±3.90	42.2±21.5	131±11	1, 2
NGC 3516	7.76±2.65	42.7±14.6	164±35	5
NGC 3783	5.42±0.99	29.8±5.4	95±10	1
NGC 4051	0.348±0.142	1.91±0.78	84±9	2, 4
NGC 4151	2.42±0.83	13.3±4.6	93±14	4
NGC 4593[c]	$0.98^{+1.70}_{-1.26}$	$5.36^{+9.37}_{-6.95}$	124±29	2
NGC 5548	12.20±0.47	67.1±2.6	183±27	4
NGC 7469	2.21±0.25	12.2±1.4	152±16	1

[a]From Peterson et al. (2004).

[b]Scaled using $f = 5.5$.

[c]Excluded from fits.

References. — (1) This work; (2) Nelson & Whittle 1995; (3) Green et al. 2003; (4) Paper I; (5) Arribas et al. 1997.

Table 4. M_{BH}–σ_* Fitting Results

Constraint	Slope (β)	Intercept (α)	χ^2_ν	$\langle f \rangle$
F02 slope	4.58	7.48±0.13	2.90	5.5±1.9
T02 slope	4.02	7.39±0.12	2.87	5.5±1.7
none	4.11±1.07	7.40±0.21	3.11	N/A
F02 slope, no NGC 4051	4.58	7.50±0.14	3.09	5.2±1.9
T02 slope, no NGC 4051	4.02	7.42±0.12	2.96	5.1±1.6